# Some thoughts about scanning probe microscopy, micromechanics, and storage

by D. W. Pohl

**Interaction and actuation mechanisms used in scanning probe microscopies (SPM) have inherent potential for storage applications, but many unresolved conceptual and technical questions have precluded a thorough assessment of this potential so far. However, the intrinsic properties of SPM instrumentation and tip/sample interactions allow a number of important parameters and their ultimate values to be estimated. Coping with and possibly surpassing established technologies will require massive parallelism of SPM-type recording heads, a condition that might be satisfied in an elegant manner by using SPM-type, *circulating* piezoelectric flexural actuators. Operation of an entire array of recording heads will require highly precise micromechanical manufacturing and/or sophisticated control mechanisms. The resulting tolerance requirement can be relaxed by choosing long-range SPM interactions (Coulomb forces, capacitance, near-field optics, etc.). Furthermore, the interaction must allow a high recording speed. The restriction to read-only storage can facilitate exploratory work; the writing process in this case might be replaced by replication, similar to the techniques used in the production of compact disks.**

## 1. Introduction

Imaging an object with a scanning probe is equivalent to the *reading* of information; the ability to modify locally allows one to *write* data. Scanning probe microscopies (SPM) have both capabilities and are therefore principally of interest also for storage applications. Hypothetical SPM-based storage devices would fall into the category of *direct-access storage devices (DASD)*, where tip, sample, and scanner correspond to recording head, disk, and disk drive, respectively. The name *nanoDASD* is used here to emphasize the potential for submicron-bit-size performance.

NanoDASDs, to be of practical interest, would have to outperform compact disks (CD-ROM, with a "*nanoCD*" as storage element) or magnetic storage devices, or at least hold strong promise to do so in the future. To be more specific, nanoDASD would have to be superior to established technology in at least one important property such as access time—without significant loss in other

©Copyright 1995 by International Business Machines Corporation. Copying in printed form for private use is permitted without payment of royalty provided that (1) each reproduction is done without alteration and (2) the *Journal* reference and IBM copyright notice are included on the first page. The title and abstract, but no other portions, of this paper may be copied or distributed royalty free without further permission by computer-based and other information-service systems. Permission to *republish* any other portion of this paper must be obtained from the Editor.

0018-8646/95/$3.00 © 1995 IBM

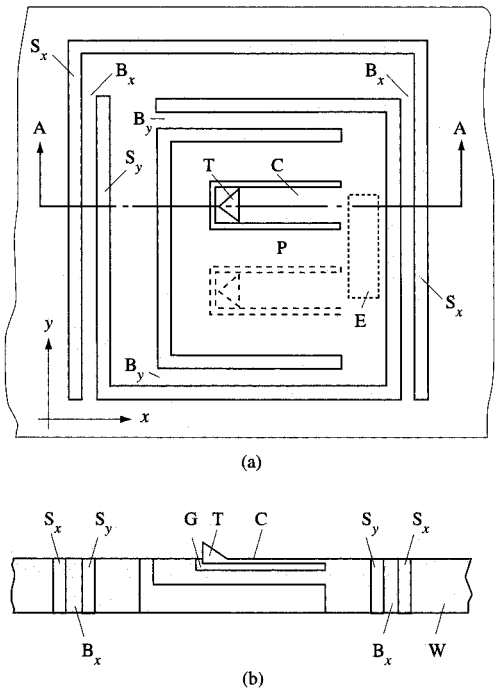


**Figure 1**

Proposed micromechanical STM (from [12]). (a) Top view, (b) side view. Micromechanical cantilever C with tip T can be deflected electrostatically by applying voltage across gap G. Slots $S_x$ and $S_y$ in the silicon wafer leave thin cantilever-like beams $B_x$ and $B_y$, which allow lateral deflection of platform P with respect to the rest of the wafer W. The second cantilever (dashed lines) indicates the possibility of operating several tips in parallel. E might be the location of on-chip electronic circuitry. The entire STM, including the inner part (P), can be manufactured from a commercial silicon wafer using known micromechanical techniques [32].

parameters. This is a formidable task in view of the present standards and the progress to be expected in the years to come. With our present knowledge, it is difficult to foresee whether nanoDASD ever will have a chance—but it is also *too early to rule out this possibility entirely.*

The intention of this paper therefore is to examine SPM technology from the point of view of storage technology requirements, to discuss necessary modifications and possible optimizations, and thus to provide some guidelines for more specific exploration. *Note that this paper is by no means intended as a complete assessment of nanoDASD, and even less as a proposal of a viable alternative to established technology; its sole purpose is to show some of the features of SPM techniques that, beyond arguments merely concerning bit size, might be of interest in the context of storage technology.*

## 2. General considerations

As its main feature, the enormous resolving power of SPM holds promise for very small bit size and very high storage density. This had already been recognized in the early days of SPM; see, for instance, the review by Quate [1] and the references cited therein. Information may be stored in topographic form (small craters [2–5] or mounds [6]), structural changes (amorphous/crystalline) [7], local electric charging [8], or magnetized domains [9]. This paper builds primarily on the author's own investigations and on those of a number of collaborators in this area, which began soon after the birth of scanning tunneling microscopy (STM) in 1981. A large part of our storage-related work has been documented as patents [10–17].

To estimate the possible performance of a nanoDASD, a bit size of 30 nm has been chosen. This value may be considered reasonable with regard to the resolution of the various SPM techniques as well as to the forthcoming requirements of storage technology. The 30 nm, of course, may not be achieved right from the beginning of experimentation, nor should this be considered the ultimate limit of bit size. It is further assumed that information is transferred to the storage medium by *replication of a master disk*, which has proven very successful in CD-ROM technology. This implies that replication techniques such as embossing, injection molding, or stamping can be extended into the sub-100-nm regime—and there is no reason why this could not be done. Embossing and injection molding of submicron-sized structures actually are already being used in mass production of holograms for identification purposes (e.g., on credit cards) [18–20]. In addition, stamping techniques were demonstrated recently to transfer submicron-sized structures using solutions of alkanethiolates and related compounds. These molecules have the property to self-assemble as monolayers (SAM) on metals such as silver or gold [21, 22]. Such replication techniques may become instrumental in the mass production of forthcoming nanometer-structured products.

Various design considerations indicate a need for parallel operation of many reading heads in a nanoDASD, each of them interrogating only a small fraction of the storage area. This requires precise structuring on a microscopic scale, a task that can be mastered best with the methods of micromechanics. A few aspects are discussed in Section 3.

The relative motion between recording head and storage medium in a nanoDASD could be provided by the conventional rotating disk drive (see for instance [5, 11]), and the standard aerodynamic regulation of flying height could be used for distance control. Such an approach, however, sidesteps an instrumental feature of the SPM technique, namely its *piezoelectric flexural actuator (PFA)* system. The PFA approach makes nanoDASD conceptually

different from rotating disk devices [13]. As a consequence, such a nanoDASD will have a number of interesting features not available in conventional DASD (and vice versa); in particular, it may be convenient for parallel operation of large arrays of individual recording heads.

The following considerations (and use of the term *nanoDASD*) are restricted to flexural actuation and a proposed mode of operation called *circulation*. This requires a detailed discussion of the properties of two-dimensional PFAs. A number of relevant operating and storage parameters (storage capacity, access time, and reading speed) [23] are derived in Section 4.

The organization of the storage area into "megarrays" of "microdisks" is discussed in Section 5. Section 6 is devoted to questions of gap-width (flying-height) control, which is much more demanding than in SPM, since all reading heads must be kept at operating distance simultaneously.

*Reading* may be based on the detection of tunnel currents [6], interaction forces (van der Waals, repulsive, magnetic, Coulomb) [2–5], capacity [8, 24, 25], or optical properties [7, 10, 11, 26–28]. It also might be possible to combine the magnetic interactions used so successfully in DASD technology (induction, magnetoresistance) with PFA techniques. The different reading processes correspond directly to the respective SPM imaging modes. Performance estimates can therefore be made in a semiquantitative way (Section 7). Some proposals are made regarding the selection of interaction/storage mechanisms and for the optimization of the operating characteristics.

## 3. Micromechanics: Small is stable

• *Micromechanical STM*

Mechanical stability enormously facilitates the operation of SPM—it was actually instrumental in the breakthrough of STM in the early '80s—and will be a *must* for nanoDASD as well. Reduction of size is the best way to achieve this goal [23]. The ultimate SPM might therefore be a completely [12, 29] or at least partially [16, 30, 31] micromechanical device.

An early proposal for a micromechanical STM is shown in **Figure 1** [12]. The instrument utilizes a small cantilever with tip (similar to the ones now common in force microscopy), which allows gap-width regulation by bending. Elastic beams oriented normal to the chip surface allow lateral motion. Deflection might be achieved with electrostatic forces, but the recently developed thin-film piezoelectric bimorph technique [29] may be more efficient.

• *Micromechanical nanoDASD head*

For storage applications, both the deflection (scan) range and the speed of a flexural actuator should be as large as possible in order to maximize storage capacity and bit rate, respectively. These are two contradictory conditions that

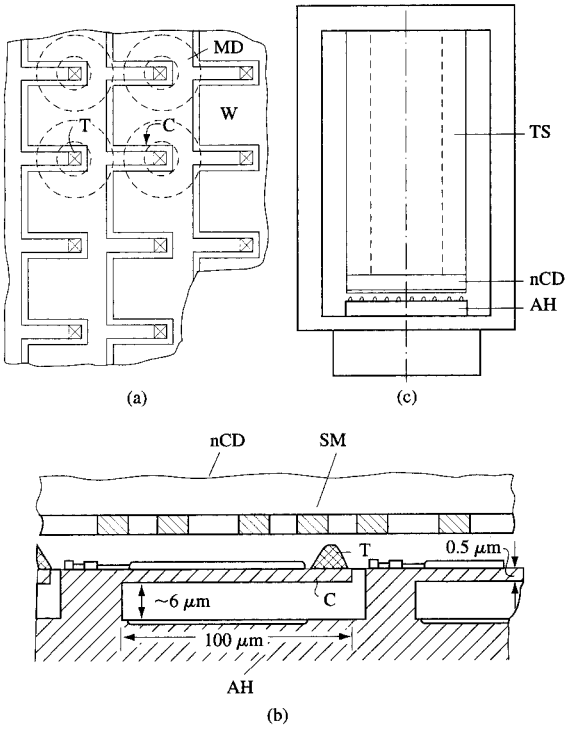


**Figure 2**

Proposed parallel operation of many SPM-like probes forming the *array head* (adapted from [13]). (a) Top view and (b) side view show individual probes (tips) T at the ends of elastic cantilevers C residing at the surface of base W. The dashed circles MD in (a) symbolize four *microdisks* on the surface of the nanoCD. The side view (b) sketches both array head AH (bottom) and *nanoCD* nCD (top) with a layer of bits written into the storage medium SM. (c) The nanoCD may be mounted in juxtaposition to the array head on the end face of a tube scanner TS. The latter, combined with a means for orientational alignment (not shown), provides average distance control and lateral (circulatory) motion. The cantilevers allow individual distance control.

cannot be satisfied simultaneously with the available PFA technology. Parallel operation of many SPM-type subunits is therefore a necessity, and can readily be implemented with two-dimensional PFAs, which allow translation in both lateral directions (cf. the subsequent section on circulation with PFAs).

Efficient use of the available storage area requires that the individual subunits be spaced at distances equal to the deflection range. The nanoDASD head disk assembly (*nanoHDA*) consequently consists of an array recording head (*array head*) having the global shape of a flat disk (instead of the sharply pointed SPM "tip") and an appropriately patterned storage disk (*nanoCD*) [13] [**Figure 2(a)**]. The functional surfaces of array head and

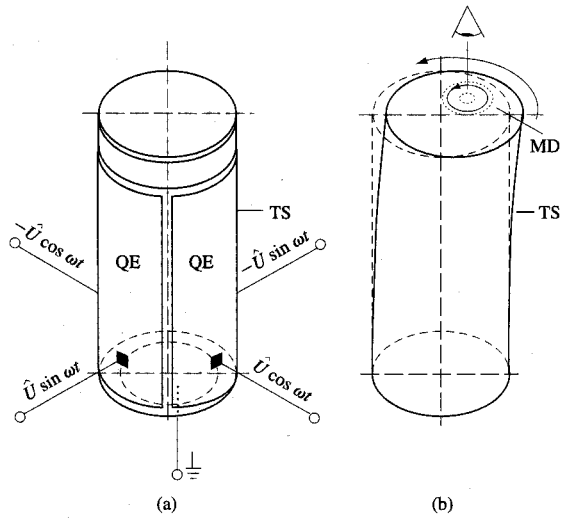


**Figure 3**

Principle of *circulation*, example of a tube scanner, from [13]: (a) ac voltage is applied to the four quadrant electrodes QE (only two of them are visible) of tube scanner TS with progressing $\pi/2$ phase shift. (b) The voltage deflects the tube such that each point of the end piece moves on a circular path. At resonance, sizable amplitudes can be maintained. The ring-shaped area MD symbolizes one *microdisk*.

nanoCD must be adjusted strictly parallel to each other, leaving a very small gap in between [**Figures 2(b)** and **2(c)**]. This introduces a severe new alignment requirement compared to SPM tip-alignment control. The nanoCD, on the other hand, can be produced to a very high degree of flatness, which is not typically the case for SPM objects.

The individual probe "tips" may be integrated into the array head, which would make them quite insensitive to wear, or they may be attached either directly (see, for instance, Figure 5 [17], shown later) or indirectly via arrays of elastic cantilevers [Figures 2(a) and 2(c)]. The latter, more complex structure would allow individual gap-width regulation, at least to some degree. Parallel operation (without feedback) of up to five cantilevers in contact-AFM mode was demonstrated recently by Minne et al. [33]. Pairs of cantilevers were used for writing structures onto amorphous silicon while scan images were created with five cantilevers simultaneously, increasing the inspection rate by this amount.

The diameter of the complete nanoHDA may be 10 to 60 mm (see the section on megarray organization), i.e., not microscopically small. Conventional "macromechanical" piezoelectric actuators may therefore be sufficient for the production of their relative lateral motion, at least in the early phases of exploration. At a later stage, more elegant but also more elaborate micromechanical actuators [29, 34] might be given preference.

## 4. Circulation: Opportunity for fast and massively parallel operation

• *Definition*

Line scanning, the standard SPM mode of operation, would be of little use for recording purposes. The required constant high-speed data flow can be achieved with two-dimensional flexural actuators, however, with an oscillating driving force that is 90° out of phase for the two directions [**Figure 3(a)**]. All points of the actuator head then describe ellipses of the same shape and size, their centers being at the position of the points at rest. Proper adjustment of the excitation amplitudes provides circular motion at a given radius $r$, as sketched in **Figure 3(b)**. For a given driving force the amplitude of circulation is largest when the actuator is excited at its (lateral) resonance frequency. This turns out to be the optimum condition of operation. The base onto which the piezotube is mounted must be carefully designed in this case because the resonance properties are influenced by the entire tube/base assembly. It should emphasized that circulation is *not a rotation* but a *translation on a circular path:* All points have equal characteristics of motion.

• *Circulation with PFAs, particularly tube scanners*

Tube scanners with quadrant electrodes are three-dimensional PFAs that allow lateral translation in the $x$- and $y$-directions by bending and axial ($z$) motion by elongation [35]. The two bending modes, cf. Figure 3, are actuated by applying voltage of opposite sign to opposite quadrants. The tube scanner responds like a bimorph, i.e., by a quadratic length dependence of the deflection amplitude. Another effective implementation utilizing this principle is a scanner consisting of four flat bimorph-piezo-elements arranged in a square [36]; compared to the tube scanner, the "square" scanner is flatter but laterally more extended.

The circulation of PFAs is subject to hysteresis and drift as the velocity vector changes continuously. Owing to the rotational symmetry, however, the only effect is a constant phase lag and some energy dissipation as long as the PFA circulates at fixed amplitude. Changes of amplitude cause hysteretic and drift effects similar to those in SPM-type line scanning that must be compensated by means of independent sensing and control mechanisms. (For the following discussion, the tube scanner is taken as an example because it is used almost exclusively in present-day SPMs.)

The most relevant tube scanner parameters for the present considerations are, besides the geometrical

dimensions (length $l$, radius $r$, and wall thickness $a$), the material constants (piezoelectric strain coefficient $d_{31}$, velocity of longitudinal sound $c_l$, quality factor $Q$ of the lowest-order bending resonance), and the maximum permissible values for the mechanical strain $u_{max}^{(mec)}$ (fracture limit) and the electric field $E$ (or voltage $U$), for which the coercive field $E_c$ (depolarization limit) is a characteristic quantity. Typical values for these quantities [37–42] used in the numerical estimates in the next section are listed in **Table 1.**

**Table 1** Characteristic data of typical piezoelectric ceramic tube scanner.

| *Geometry* | | *Material* | | *Limits* | |
|---|---|---|---|---|---|
| $l$ | 25.0 mm | $d_{31}$ | $2 \times 10^{-10}$ m/V | $u_{max}^{(mec)}$ | $2.5 \times 10^{-3}$ |
| $r$ | 3.13 mm | $c_l$ | 3000 m/s | $E_c$ | $5 \times 10^5$ V/m |
| $a$ | 0.6 mm | $Q$ | 100 | $v_{max}$ | 10 m/s |
| $f_{LOAD}$ | 0.7 | | | | |

• *Bending amplitude, bending resonance, and speed of circulation*

The *static* bending amplitude $\Delta x^{(0)}$ of a piezoelectric, thin-walled tube can be calculated from the requirement that the sum of forces and the sum of momenta be zero at any point on the tube. Under the assumption that the effects of the tube ends, the shear forces in the tube wall, and the distortion of circular cross section are negligible, the condition of mechanical equilibrium provides the expression

$$\Delta x^{(0)} \simeq \left(\sqrt{2}/\pi\right) d_{31} E (l^2/r) = \left(\sqrt{2}/\pi\right) d_{31} U (l^2/ra) \rightarrow (30 \text{ nm/V}) U. \quad (1)$$

The numerical value which follows the arrow is obtained from the data of Table 1, which are also the basis of all subsequent estimates. Here $d_{31}E$ represents the lateral strain induced in a *planar* sheet of piezoelectric material. Interestingly, the maximum piezoelectric strain $u_{max}^{(0)}$ for which the coercive field $E_c$ may be taken as a measure, i.e., $d_{31}E_c$, is roughly constant for many common piezoelectric materials (see for instance [37, 41, 42]):

$$u_{max}^{(0)} = d_{31} E_c \simeq 10^{-4}. \quad (2)$$

The maximum electrostatically allowed deflection is hence

$$\Delta x_{max}^{(0)} = \left(\sqrt{2}/\pi\right) u_{max}^{(0)} l^2/r \simeq 0.5 \times 10^{-4} \times (l^2/r) \rightarrow 10 \ \mu\text{m}. \quad (3)$$

At *resonance* the bending amplitude $\Delta x^{(r)}$ exceeds $\Delta x^{(0)}$ by the quality factor $Q$, which can be as large as 1000. (The slight difference in the bending profiles for static and dynamic excitation is ignored.) This would allow very large amplitudes even with the more moderate $Q$ value chosen in Table 1, but the fracture limit restricts the maximum strain to $10^{-3}$ and $10^{-2}$ for tensile and compressive stress, respectively [37]. Because the tube can be preloaded, we allow an intermediate value

$$u_{max}^{(mec)} = 2.5 \times 10^{-3}, \quad (4)$$

which results in

$$\Delta x_{max}^{(mec)} \simeq 0.5 u_{max}^{(mec)} l^2/r \rightarrow 250 \ \mu\text{m}. \quad (5)$$

This value is achieved in our example with an applied field of $E_{max} = 2 \times 10^5$ V/m $= E_c/4$ or $U_{max} = 90$ V.

The bending resonance frequency can be determined from the elementary cantilever equations [43], using the moment of inertia of the ring-shaped tube cross section. For the sake of brevity, the bending resonance frequency $\omega^{(r)}$ is derived for the unloaded tube only. Attachment of the array head or nanoCD to the tube end reduces $\omega^{(r)}$ roughly in proportion to the ratio of array head and tube masses. The effect of the load is accounted for by a factor of $f_{LOAD}$ heuristically assumed to be 0.7:

$$\omega^{(r)} = \left(1.875^2/\sqrt{2}\right) f_{LOAD} c_l r/l^2 \simeq (7500 \text{ m/s}) f_{LOAD} r/l^2 \rightarrow 2\pi(4 \text{ kHz}). \quad (6)$$

Note that both $\Delta x^{(r)}$ and $\omega^{(r)}$ vary with $l^2/r$, but in inverse ways. Their product is hence independent of tube shape; it represents the *speed of circulation*:

$$v^{(r)} = \Delta x^{(r)} \omega^{(r)} = (1.875^2/\pi) f_{LOAD} c_l Q d_{31} E \simeq f_{LOAD} c_l Q d_{31} E. \quad (7)$$

The maximum speed of circulation of an unloaded tube is a constant for a given field and cannot be increased by changing the tube dimensions [23]:

$$v_{max}^{(r)} \simeq c_l u_{max}^{(mec)} \simeq 10 \text{ m/s}. \quad (8)$$

The size of $v_{max}^{(r)}$ is similar to that of rotational disk drives:

$$v_{rot} \simeq 10 \text{ to } 30 \text{ m/s}. \quad (9)$$

At maximum speed, the individual probes of the array head may have to read data at a rate of at least $10^8$ bits/s.

The high speed at resonance implies a correspondingly large acceleration ($a$). As a consequence, sizable inertial forces ($F$) act on the PFA during operation. Maximum values are

$$a_{max}^{(r)} = v_{max}^{(r)} \omega^{(r)} \rightarrow 2.5 \times 10^5 \text{ m/s}^2. \quad (10)$$

The resulting force produces the strain $u_{max}^{(mec)}$ introduced at the beginning of these considerations. With an effective

mass of about 1 gram (the total mass of the piezoelectric tube is 2.3 g in our example), the maximum force reaches almost 60 newtons, corresponding to the weight of a 6-kg mass. The mounting of the piezoelectric tube hence requires careful design. Tube and mount in fact must be considered as an entity the elastic properties of which must be optimized. The motion of the tube or, generally speaking, of the PFA can be decoupled from the mount to a large extent if higher-order bending modes are excited and the tube is supported at the oscillation nodes. To arrive at the performance assumed in our example, the tube has to be considerably longer in this case.

An essential difference between a PFA and a conventional disk drive is the *angular* speed: In our example, the resonance occurs at 4 kHz, which corresponds to 240000 rpm and a latency of 250 $\mu$s. The fastest rotational disk drives, on the other hand, operate at about 10000 rpm. The price for the dramatic increase is a similarly dramatic reduction in disk radius, i.e., from a few inches in diameter of standard magnetic disks to 250 $\mu$m in our case. It is possible, of course, to make other trade-offs between radius and angular velocity.

Track changes, i.e., changes in the circulation amplitude $\Delta x$, can be provoked fastest by increasing the driving voltage amplitude to the maximum level allowed, $U_{\text{pulse}} \simeq aE_c$, with the appropriate phase. The growth of the PFA circulation amplitude follows the laws governing the buildup of a resonant oscillation. Since $E_{\max} = E_c/4$ only, it is justified to linearize the principally exponential curve of amplitude growth (decrease), which results in

$$\frac{\Delta x}{\Delta x_{\max}^{(\text{mec})}} = \frac{1}{2}\left(\frac{\Delta x_{\max}^{(0)}}{\Delta x_{\max}^{(\text{mec})}}\right)\omega^{(r)}t \rightarrow 0.02\omega^{(r)}t = \frac{t}{(2\text{ ms})}. \quad (11)$$

Hence, the maximum possible amplitude change, start-up from zero to $\Delta x_{\max}^{(\text{mec})}$, takes 2 ms; switching between adjacent tracks can be maintained within less than one period of circulation. Even faster track changes could in principle be achieved using variable compliance arrangements not considered here. As mentioned in the section on circulation with PFAs, hysteresis and creep may play a disturbing role during track change, requiring independent radial position control for accurate track addressing.

## 5. Ideas on *micro*disk and *mega*array organization

- *Microdisk*

It is immediately obvious from the above data that the operating characteristics of nanoDASDs would differ greatly from those of conventional DASD devices. This will require new architectures but may also open new opportunities. The small amplitudes of circulation demand massively parallel operation, as mentioned before, in order to provide sufficient storage capacity. The large angular speed, on the other hand, opens the opportunity for extremely short on- and off-track search times.

With a circulated array head, each individual head can interrogate a circular ring-shaped area ["microdisk," Figures 2(a) and 3(b)] whose outer radius must not exceed the maximum amplitude $\Delta x_{\max}$ of the actuator. The individual microdisks may be organized similarly to established rotating disk technology. In particular, a minimum radius $\Delta x_{\min}$ is to be introduced which will limit the usable storage area to some (large) fraction of the microdisk area. The value of $\Delta x_{\min}$ depends on architectural and engineering considerations in the first place. Assuming, for example, $\Delta x_{\min} = 0.5\Delta x_{\max}$, the maximum disk area is

$$A_{\max} = (3/4)\pi\Delta x_{\max}^2 \rightarrow 0.15\text{ mm}^2. \quad (12)$$

With a bit size of 30 nm and a track distance of 100 nm, the microdisk can accommodate 1250 tracks with an average of about 40000 bits per track, corresponding to a storage capacity of 5 MB. The small number of tracks is advantageous for track alignment, but the storage capacity of the individual microdisk is clearly too small to be considered for practical applications.

- *Megarray organization*

The total storage capacity of a nanoCD, in order to be of interest for practical application, should be of the order of, say, 5–50 GB; this requires arrays of size 32 × 32 to 128 × 128. The total storage area will hence cover an area of 16 mm × 16 mm (64 mm × 64 mm) for the assumed bit size of 30 nm × 100 nm. The size of such arrays is convenient for addressing 32-, 64-, or 128-bit buses directly. For this purpose it is necessary to integrate head multiplexers which interleave the data from the individual columns of the array for each line. For large arrays, the implementation of multiplexing electronics into an array head is by no means trivial.

## 6. Regulation of gap width (flying height)

The nanoHDA with array architecture requires more sophisticated gap-width regulation than an SPM because *all* elements must be maintained at interaction distance. The operating gap width should be less than the bit size to avoid crosstalk, *and* sufficiently small to ensure detectable interaction between the probes (heads) and the storage medium. For the 30-nm bit diameter envisaged in our example, the gap hence should not exceed 10–20 nm, which would allow for tolerances of 3–6 nm, or "$\lambda$/200 to $\lambda$/100" in the language of opticians.

• *Parallel plates/global regulation*

*Flatness* of up to λ/200 is in fact commercially available, for instance for high-quality interferometric mirrors over areas as large as 100 mm in diameter [44]; even lower is the surface *roughness* of standard optical elements [45]. Array heads and nanoCDs with such a flatness in principle allow for a rigid parallel-plate setup. Three distance sensors and three actuators are sufficient, in principle, to control the gap width (flying height) in an active way. Alternatively, passive techniques similar to those used in conventional rotating disk DASDs might be employed. The stiff parallel-plate arrangement is limited to long-range interactions such as near-field optical interactions, Coulomb or magnetic forces, or capacitive sensing, but it has the advantage of being relatively simple once the tolerance problem has been mastered. At the required high degree of flatness, precautions against adhesive sticking will have to be taken. Appropriate surface passivation, for instance with hydrophobic thin films, may help stabilize the gap width at the desired distance.

• *Cantilever arrays/individual regulation*

Tunneling and "atomic" force interactions require operating distances in the subnanometer regime, which can be maintained only by individual gap-width regulation. In this case, the recording elements can be mounted on miniaturized elastic deflectors which can be actuated by appropriate application of voltage [Figure 2(b) and **Figure 4**]. Control circuitry can be installed for each head if micromechanical and microelectronic techniques are combined in the probe head.

The complexity of the necessary control circuits can be reduced if the concept of perfect closed-loop feedback regulation generally used in SPM is forsaken in favor of open-loop "feed-forward" circuitry which compensates distance variations incompletely. Figure 4(b), as an example, shows an arrangement consisting of one resistor, one capacitor, and one FET in the path of a tunnel current [15]. Combined with electrostatic or piezoelectric cantilever deflection, the scheme can reduce gap-width variations from 1:1 in unregulated operation to about 1:30. Similar schemes may be conceived for other types of interaction such as forces, charges, or optical near fields.

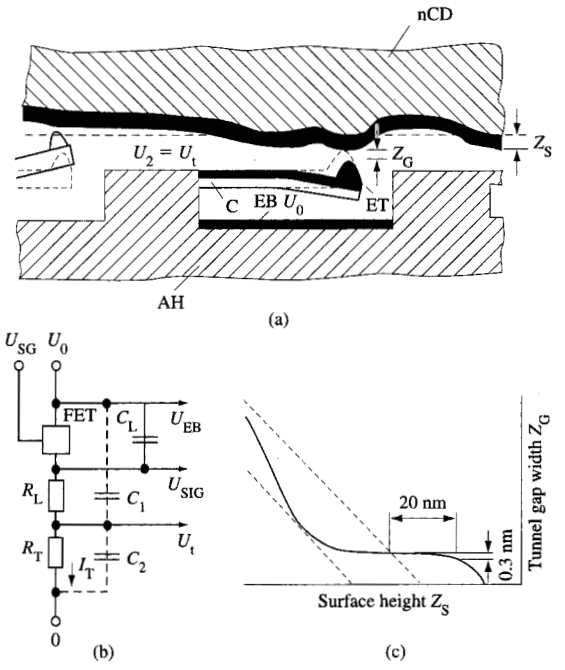


**Figure 4**

Proposed "feed-forward" distance control for tunnel junctions (adapted from [15]). (a) Distance between the individual probes of the array head AH *at rest* and the surface of the storage medium undergoes variations $Z_S$ during circulation due to finite roughness. (b) The circuit consisting of one FET, one capacitor ($C_L$) and one resistor ($R_L$), in series with tunnel resistance ($R_T$), compensates variations of $Z_S$ by a corresponding deflection of cantilever C. For this purpose, $U_0$ and $U_t$ are connected to electrodes EB and ET, respectively, while the storage medium is at bias level. C is deflected in proportion to the counteracting electrostatic forces generated by $(U_0 - U_t)$ and $U_t$. Upon approach, the decreasing tunnel resistance in combination with the flat *I/V* characteristic of the FET causes a strong decrease of $U_t$, resulting in retraction of the cantilever until the system is in balance again. A tunnel signal $U_{SIG}$, assumed to be rapidly varying, can be measured across $R_L$. (c) With proper layout, the $Z_G/Z_S$ characteristic has a plateau that allows for sizable manufacturing tolerances. The numbers (20 nm/0.3 nm) refer to an example explained in [15].

## 7. Interaction mechanisms

The different known SPM interactions can now be examined in the light of the (electro-) mechanical properties of the nanoDASD discussed in the preceding sections. A certain selection may be made on the basis of data rate, gap width, and complexity requirements.

• *Tunneling*

The *first* of all SPM techniques would clearly excel in terms of bit size, but requires extremely careful distance control. The principal problem with tunneling, however, is the speed of detection, which is limited by the large impedance of the tunnel junction and its capacitance. The minimum practicable response time may be of the order of 1 μs, but even this value has not yet, to the author's knowledge, been verified experimentally.

• *Forces*

The detection process is based on mechanical deformation of an elastic element, in general a small cantilever. When operated in the attractive, *noncontact* mode, the deflection

requires a minimum time span of several periods of oscillation at the relevant resonance frequency. The response time $\delta t$ is considerably reduced in the *contact* mode by application of a loading force $F_L$ [46],

$$\delta t \simeq 2\sqrt{m_{eff} h / F_L}, \tag{13}$$

where $m_{eff}$ and $h$ are the effective mass of the cantilever and the depth of a pit representing one bit. Equation (13) holds under the assumption that the deflection of the free cantilever under the influence of $F_L$ would be large compared to $h$. In order to arrive at a fast response, the cantilever should be as small as possible and the load as large as possible; the latter, however, has to be kept quite small in order to avoid problems of wear. Indeed, by reducing the dimensions of their cantilevers, Mamin et al. [46] were recently able to demonstrate data rates in excess of 1 Mb/s with a contact-mode AFM scheme. Electric or magnetic interaction forces, on the other hand, are detected in noncontact mode and hence require more time for signal acquisition.

- *Capacitance*

Capacitance measurements can be made sensitively and at high speed by means of high-frequency electronic circuitry. The capacitance sensor of RCA [47], for instance, operates near 1 GHz, allowing response times well in the submicrosecond regime. The ability of such sensors to detect and scan-image trapped charges in a $Si_3N_4$ film via a shift in the depletion voltage of Si was demonstrated by Iwamura et al. [48] and more recently by Barrett and Quate [8, 24], as well as by Terris and Barrett [25]. The operating distance should be kept as small as possible, since the capacitance differences measured between depletion and accumulation states are reduced dramatically with increasing gap width. The smallest bit size was 75 nm [8]. A problem might exist in the necessary sophisticated detection circuitry; a considerable effort would be required to implement (32 × 32) or more such circuits into an array head.

- *Light*

*Scanning near-field optical* microscopy (SNOM) has a demonstrated resolution capability of about 30 nm [10, 26–28, 49]. Gap widths of the order of 10 nm are convenient. The detection response time can be extremely fast, being limited only by the number of photons available per bit. With present SNOM techniques, about $10^{-6}$ of the incident light power is coupled through a 50-nm aperture, and the input light flux is limited to ≃10 mW, owing to heating effects. Novotny et al. recently showed that the transmission can be improved by several orders of magnitude if the cone angle of the light guide is increased sufficiently [50]. Moreover, the thermal stability can be raised by at least one order of magnitude. Hence, it appears that near-field optical (NFO) signal levels of more than $10^5$ photons/μs (currently about 100) can be achieved in the future, which would allow a reading speed of about $10^7$–$10^8$ bit/s.

Read-out of bits from magneto-optic [28, 51] and phase change media [7] has already been demonstrated with a minimum bit size of 70 nm. The optical effects associated with these phenomena are fairly weak, however, which seriously limits the reading speed.

For read-only purposes (nanoCD), information could be stored in the form of little indentations or patches of a material different from that of the substrate. Such structures can be generated with the replication techniques mentioned in Section 2. They cause light scattering, which can be used for reading [14, 51–53]. Metal/nonmetal combinations are particularly efficient because the large differences in dielectric constant result in strong light-scattering effects. A possible implementation of a near-field optical nanoCD is shown in **Figure 5** [17].

A major advantage of NFO is that the near-field interaction and the detection process can be separated physically and therefore optimized individually. Moreover, the electronic circuitry required is fairly simple and commercially available. It is possible, for instance, to project the light emerging from the individual probes of the array head onto the elements of a CCD array. The latter automatically provides sequential read-out.

## 8. Summary

The techniques developed for SPM hold potential for extension to storage applications because

1. The various interaction mechanisms, combined with SPM-like probes, may allow reading and, to a restricted extent, writing/erasing of bits of very small physical size.
2. The PFA instrumentation used in SPM may allow very fast data access and, combined with arrays of recording heads, massively parallel operation.

These two independent aspects make possible three different strategies for the development of SPM-derived storage devices:

1. SPM-type recording + conventional disk drive (rotation).
2. Conventional recording + PFA disk drive (circulation).
3. SPM-type recording + PFA disk drive (circulation).

The third possibility offers the prospect of operating conditions that are qualitatively different from the established ones. This was therefore made the main issue of the present paper. The discussion was restricted to

read-only, CD-ROM-type storage (*nanoCD*) because replication techniques might well be extended into the sub-100-nm regime. Furthermore, with this restriction, the entire issue of SPM-type storage can be presented in a more comprehensive way.

The analysis and numerical estimation of the characteristic parameters of PFAs led to the definition of optimum operating conditions (*circulation*) and to the requirement of parallel operation (*array head*). As a consequence, regulation of the "flying height" becomes a major issue. It is necessary either

1. to mount the heads on individually controllable actuators and implement control electronics for each head, or
2. to produce array heads and *nanoCDs* with such a degree of flatness and precision that all heads can be kept at operating distance by global alignment.

The first solution allows the very small gap-width operation necessary for tunneling/atomic forces. It promises an extremely small bit size, but it requires the integration of complex mechanical and electrical circuitry in the array head. The second approach is feasible if the tolerances in head/disk distance are sufficiently large, i.e., for "long-range" (10–100-nm) SPM interactions such as near-field optical effects, capacitance, magnetic and electric (Coulomb) forces. In both cases, massive usage of micromechanics and other microstructuring techniques will be required.

"Long-range" SPM interactions allow bit sizes of 30–100 nm in diameter, which is about ten times better than what can be achieved with present techniques, but worse than what can be achieved by exploiting tunneling (STM) or contact forces (AFM). "Long-range" interactions still offer the attractive prospect of a $10^{11}$–$10^{12}$-bit/in.$^2$ storage density. The number of SPM-type interactions suitable for storage applications is also restricted by the necessary data rates, well above $10^6$ bits/s per individual head, corresponding to a (maximum) response time of $<1$ $\mu$s. This requirement can be satisfied by *contact force, capacitance*, and *near-field optical recording*. The "NFO" nanoCD might be developed from existing CD technology.

A good deal of dedicated exploratory work as well as the development of new concepts is still needed to assess fully the potential of storage devices based on SPM techniques.

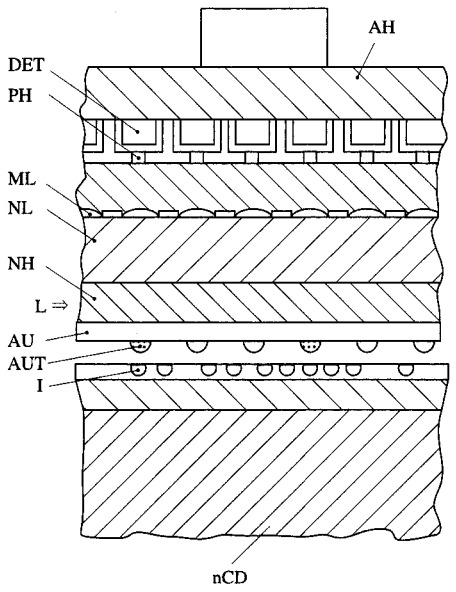


**Figure 5**

Proposed near-field optical nanoCD player (from [17]). The array head (top) consists of a planar optical waveguide (NL: low; NH: high index of refraction; AU: gold film) to which an array of small gold particles ("tips") AUT is attached as optical probes. The fundamental waveguide mode is excited by a light source L on the left-hand side. The parameters may be chosen such that a plasmon can be excited at the gold particles. The plasmon makes itself felt by strong light scattering. The plasmon resonance is highly sensitive to changes of the environment. Therefore, if an indentation I in the surface layer of the nanoCD passes under the particle, a strong variation of the scattering intensity is produced. Preliminary experiments indicated a resolution of about 50 nm [53]. The scattered radiation is directed onto an array of detectors DET by means of corresponding arrays of microlenses ML and pinholes PH. The detector array might be part of a CCD. The arrangement shown is merely one of a variety of similar possible implementations.

## References and note


1. C. F. Quate, "Surface Modification with the STM and the AFM," *Scanning Tunneling Microscopy and Related Methods*, R. J. Behm, N. Garcia, and H. Rohrer, Eds., *NATO ASI Series E: Applied Sciences*, Kluwer, Dordrecht, 1990, Vol. 184, pp. 281–297.
2. David W. Abraham, H. Jonathon Mamin, Eric Ganz, and John Clarke, "Surface Modification with the Scanning Tunneling Microscope," *IBM J. Res. Develop.* **30,** 492–499 (1986).
3. H. van Kempen and G. F. A. van de Walle, "Applications of a High-Stability Scanning Tunneling Microscope," *IBM J. Res. Develop.* **30,** 509–514 (1986).
4. H. J. Mamin and D. Rugar, "Thermomechanical Writing with an Atomic Force Microscope Tip," *Appl. Phys. Lett.* **61,** 1003–1005 (1992).
5. S. Hoen, H. J. Mamin, and D. Rugar, "Thermomechanical Data Storage Using a Fiber Optic Stylus," *Appl. Phys. Lett.* **64,** 267–269 (1994).
6. H. J. Mamin, P. H. Guethner, and D. Rugar, "Atomic Emission from a Gold Scanning-Tunneling-Microscope Tip," *Phys. Rev. Lett.* **65,** 2418–2421 (1990).
7. S. Hosaka, T. Shintani, M. Miyamoto, A. Hirotsune, M. Terao, M. Yoshida, S. Honma, and S. Kammer,

"Scanning Near-Field Optical Microscope with Laser Diode and Nanometer-Sized Bit Recording," *Thin Solid Films* (1995, in press); S. Hosaka, S. Hosoki, T. Hasegawa, W. Koyanagi, T. Shintani, and M. Miyamoto, "Fabrication of Nanostructures Using Scanning Probe Microscope," *J. Vac. Sci. Technol. B* **13** (1995); Sumio Hosaka, Toshimichi Shintani, Mitsuhide Miyamoto, Akemi Hirotsune, Motoyasu Terao, Masaru Yoshida, Kouichi Fujita, and Stefan Kammer, "Nanometer Sized Phase Change Recording Using a Scanning Near-Field Optical Microscope with a Laser Diode," *Jpn. J. Appl. Phys.* **35** (1B, part 1) (1996, in press).

8. R. C. Barrett and C. F. Quate, "Charge Storage in a Nitride–Oxide–Silicon Medium by Scanning Capacitance Microscopy," *J. Appl. Phys.* **70,** 2725–2733 (1991).
9. Y. Martin and H. K. Wickramasinghe, "Magnetic Imaging by 'Force Microscopy' with 1000 Å Resolution," *Appl. Phys. Lett.* **50,** 1455–1457 (1987).
10. D. W. Pohl, "Optical Near-Field Scanning Microscope," European Patent 0112401 (filed December 27, 1982; application published July 4, 1984); U.S. Patent 4,604,520, August 5, 1986.
11. J. G. Bednorz, W. Denk, M. Lanz, and D. W. Pohl, "Light Waveguide with a Submicron Aperture, Method for Manufacturing the Waveguide and Application of the Waveguide in an Optical Memory," European Patent 0112402 (filed December 27, 1982; application published July 4, 1984); U.S. Patent 4,684,206, August 4, 1987.
12. J. K. Gimzewski and D. W. Pohl, "Scanning Tunneling Microscope," European Patent 0194323 (filed March 7, 1985; application published September 17, 1986); U.S. Patent 4,668,865, May 26, 1987.
13. D. W. Pohl, U. T. Duerig, and J. K. Gimzewski, "Direct Access Storage Unit," European Patent 0247219 (filed May 27, 1986; application published December 2, 1987); U.S. Patent 4,831,614, May 16, 1989.
14. U. T. Duerig, U. Ch. Fischer, and D. W. Pohl, "Sensor for Converting a Distance to Optical and Further to Electrical Energy, and Surface Scanning Apparatus Using the Same," European Patent 0308537 (filed September 25, 1987; application published March 29, 1989); U.S. Patent 5,025,147, June 18, 1991.
15. D. W. Pohl and C. Schneiker, "Distance-Controlled Tunneling Transducer and Direct Access Storage Unit Employing the Transducer," European Patent 0363550 (filed October 14, 1988; application published April 18, 1990); U.S. Patent 5,210,714, May 11, 1993.
16. U. T. Duerig, J. K. Gimzewski, J. Greschner, D. W. Pohl, and O. Wolter, "Micromechanical Atomic Force Sensor Head," U.S. Patent 4,806,755, February 21, 1989.
17. D. W. Pohl, "High-Density Optical Data Storage Unit and Method for Writing and Reading Information," European Patent Application 0568753 (filed May 7, 1992; application published November 10, 1993).
18. *Holography Market Place*, B. Kluepfel and F. Ross, Eds., Ross Publishers, Berkeley, CA, 1994.
19. M. T. Gale, "Diffractive Microstructures for Security Applications," *IEE Conf. Publ. Lond.* **342,** 205–209 (1991).
20. M. T. Gale, L. G. Baraldi, and R. E. Kunz, "Replicated Microstructures for Integrated Optics," *Proc. SPIE* **2213,** 2–10 (1994).
21. A. Kumar, H. Biebuyck, and G. M. Whitesides, "Patterning Self-Assembled Monolayers: Applications in Materials Science," *Langmuir* **10,** 1498–1511 (1994).
22. J. L. Wilbur, H. Biebuyck, J. C. MacDonald, and G. M. Whitesides, "Scanning Force Microscopies Can Image Patterned Self-Assembled Monolayers," *Langmuir* **11,** 825–831 (1995).
23. D. W. Pohl, "Some Design Criteria in Scanning Tunneling Microscopy," *IBM J. Res. Develop.* **30,** 417–427 (1986).
24. R. C. Barrett and C. F. Quate, "Large-Scale Charge Storage by Scanning Capacitance Microscopy," *Ultramicrosc.* **42–44,** 262–267 (1992).
25. B. D. Terris and R. C. Barrett, "Data Storage in NOS: Lifetime and Carrier-to-Noise Measurements," *IEEE Trans. Electron Devices* **42,** 944–949 (1995).
26. D. W. Pohl, W. Denk, and M. Lanz, "Optical Stethoscopy: Image Recording with Resolution $\lambda/20$," *Appl. Phys. Lett.* **44,** 651–653 (1984).
27. U. Dürig, D. W. Pohl, and F. Rohner, "Near-Field Optical Scanning Microscopy," *J. Appl. Phys.* **59,** 3318–3327 (1986).
28. E. Betzig, J. K. Trautman, R. Wolfe, E. M. Gyorgy, and P. L. Finn, "Near-Field Magnetooptics and High Density Data Storage," *Appl. Phys. Lett.* **61,** 142–144 (1992).
29. S. Akamine, T. R. Albrecht, M. J. Zdeblick, and C. F. Quate, "Microfabricated Scanning Tunneling Microscope," *IEEE Electron Device Lett.* **10,** 490–492 (1989).
30. T. R. Albrecht, S. Akamine, T. E. Carver, and C. F. Quate, "Microfabrication of Cantilever Styli for the Atomic Force Microscope," *J. Vac. Sci. Technol. A* **8,** 3386–3396 (1990).
31. T. Itoh and T. Suga, "Self-Excited Force-Sensing Microcantilevers with Piezoelectric Thin Films for Dynamic Scanning Force Microscopy," *Transducers '95—Eurosensors IX, the 8th International Conference on Solid State Sensors and Actuators, and Eurosensors*, Stockholm, Sweden, June 25–29, 1995, pp. 632–635.
32. Kurt E. Petersen, "Silicon as a Mechanical Material," *Proc. IEEE* **70,** 420–457 (1982).
33. S. C. Minne, Ph. Flueckiger, H. T. Soh, and C. F. Quate, "Atomic Force Microscope Lithography Using Amorphous Silicon as a Resist and Advances in Parallel Operation," *J. Vac. Sci. Technol. B* **13,** 1380–1385 (1995).
34. J. Brugger, N. Blanc, P. Renaud, and N. F. de Rooij, "Microlever with Combined Integrated Sensor/Actuator Functions for Scanning Force Microscopy," *Sensors & Actuators* **A43,** 339–345 (1994).
35. G. Binnig and D. P. E. Smith, "Single-Tube Three-Dimensional Scanner for Scanning Tunneling Microscopy," *Rev. Sci. Instrum.* **57,** 1688–1689 (1986).
36. P. Muralt, D. W. Pohl, and W. Denk, "Wide-Range, Low-Operating-Voltage, Bimorph STM: Application as Potentiometer," *IBM J. Res. Develop.* **30,** 443–450 (1986).
37. *VIBRIT—Piezokeramik von Siemens*, Bestellnr. 281/5035/5036 (undated catalog), Siemens AG, Zentralbereich Technik, Kunststoff- und Keramikwerk Redwitz, Bahnhofstr. 43, D-96257 Redwitz, Germany.
38. *EBL Piezoceramic Elements Lead Zirconate Titanates (PZT)* (undated catalog), STAVELEY SENSORS INC., EBL Product Line, 91 Prestige Park Circle, East Hartford, CT 06108.
39. *Modern Piezoelectric Ceramics* (undated catalog), VERNITRON PIEZOELECTRIC DIVISION, 232 Forbes Rd., Bedford, OH 44146.
40. *The Piezo Book* (undated catalog), Burleigh Instruments Inc., Burleigh Park, Fishers, NY 14443.
41. *Piezoelectric Displacement Generators—Static and Low Frequencies* (undated catalog), Channel Industries, Inc., 839 Ward Drive, Santa Barbara, CA.
42. *PIEZO*, PIEZO ELECTRIC PRODUCTS, INC., 212 Durham Ave., Metuchen, NJ 08840, 1984.
43. The theory of bending vibrations is treated explicitly in a few textbooks only. My preferred reference is an old German theoretical physics textbook: W. Weizel, *Lehrbuch der theoretischen Physik*, Springer-Verlag, Berlin, 1955, Ch. B-V, Section 2.
44. *Product Catalog Bernhard Halle Nachfolger*, in particular p. 34 (undated catalog), Bernhardt Halle Nachf. GmbH &

Co., Optical Workshop, Hubertusstr. 10-11, D-12163 Berlin, Germany.
45. *Scientific & Laboratory Products, The 1994 Newport Catalog*, Ch. 2, in particular pp. 2.3, 2.19, Newport Corporation, 1791 Deere Ave., Irvine, CA 92714.
46. H. J. Mamin, L. S. Fan, S. Hoen, and D. Rugar, "Micromechanical Data Storage with Ultralow-Mass Cantilevers," *Sensors & Actuators* **48,** 215–219 (1995).
47. J. R. Matey and J. Blanc, "Scanning Capacitance Microscopy," *J. Appl. Phys.* **57,** 1437–1443 (1985).
48. S. Iwamura, Y. Nishida, and K. Hashimoto, "Rotating Disk MNOS Device," *IEEE Trans. Electron Devices* **28,** 854–860 (1981).
49. B. Hecht, D. W. Pohl, H. Heinzelmann, and L. Novotny, "'Tunnel' Near-Field Optical Microscopy: TNOM-2," *Photons and Local Probes*, O. Marti and R. Möller, Eds., *NATO ASI Series E: Applied Sciences*, Kluwer, Dordrecht, 1995, in press.
50. L. Novotny, D. W. Pohl, and B. Hecht, "Scanning Near-Field Optical Probe with Ultrasmall Spot Size," *Opt. Lett.* **20,** 970–972 (1995).
51. T. J. Silva, S. Schultz, and D. Weller, "Scanning Near-Field Optical Microscope for the Imaging of Magnetic Domains in Optically Opaque Materials," *Appl. Phys. Lett.* **65,** 658–661 (1994).
52. U. Ch. Fischer, U. T. Dürig, and D. W. Pohl, "Near-Field Optical Scanning Microscopy in Reflection," *Appl. Phys. Lett.* **52,** 249–251 (1988).
53. U. Ch. Fischer and D. W. Pohl, "Observation of Single-Particle Plasmons by Near-Field Optical Microscopy," *Phys. Rev. Lett.* **62,** 458–461 (1989).

*Received August 4, 1995; accepted for publication October 10, 1995*

**Dieter W. Pohl** *IBM Research Division, Zurich Research Laboratory, CH-8803 Rüschlikon, Switzerland (dp@zurich.ibm.com).* Dr. Pohl is a research staff member at the Zurich Research Laboratory in Rüschlikon. His scientific work is focused on optics and scanning probe microscopies. Contributions to stimulated Brillouin and Rayleigh scattering and to the development of the transient grating technique ("forced Rayleigh scattering") in the seventies were followed in 1982 by the invention of the near-field optical microscope (SNOM, also known as NSOM), an instrument that made it possible to *break the diffraction limit in optical microscopy* for the first time (1984/85). Subsequently, in addition to long periods of managerial duties, Dr. Pohl pursued the further development of SNOM and contributed to progress made with STM and AFM techniques. He is a member of the Swiss, German, and European physical societies.